

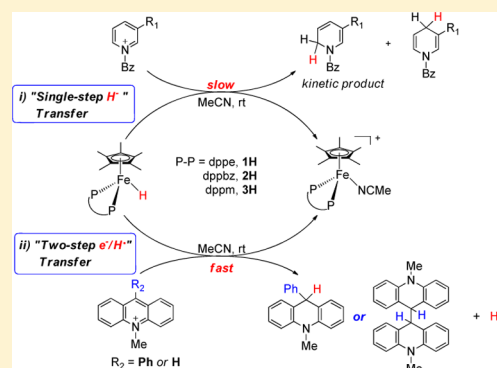
Hydride Transfer from Iron(II) Hydride Compounds to NAD(P)⁺ Analogues

Fanjun Zhang, Jiong Jia, Shuli Dong, Wenguang Wang,* and Chen-Ho Tung

Key Laboratory of Colloid and Interface Chemistry, Ministry of Education, School of Chemistry and Chemical Engineering, Shandong University, No. 27 South Shanda Road, Jinan 250100, People's Republic of China

Supporting Information

ABSTRACT: Iron(II) hydride complexes of the “piano-stool” type, Cp*(P-P)FeH (P-P = dppe (1H), dppbz (2H), dppm (3H), dcpe (4H)) were examined as hydride donors in the reduction of *N*-benzylpyridinium and acridinium salts. Two pathways of hydride transfer, “single-step H⁻” transfer to pyridinium and a “two-step (e⁻/H[•])” transfer for acridinium reduction, were observed. When 1-benzylpyridinium cation (BNA⁺) was used as an H⁻ acceptor, kinetic studies suggested that BNA⁺ was reduced at the C6 position, affording 1,6-BNAH, which can be converted to the more thermally stable 1,4-product. The rate constant *k* of H⁻ transfer was very sensitive to the bite angle of P–Fe–P in Cp*(P-P)FeH and ranged from 3.23 × 10⁻³ M⁻¹ s⁻¹ for dppe to 1.74 × 10⁻¹ M⁻¹ s⁻¹ for dppm. The results obtained from reduction of a range of *N*-benzylpyridinium derivatives suggest that H⁻ transfer is more likely to be charge controlled. In the reduction of 10-methylacridinium ion (Acr⁺), the reaction was initiated by an e⁻ transfer (ET) process and then followed by rapid disproportionation reactions to produce Acr₂ dimer and release of H₂. To achieve H⁻ transfer after ET from [Cp*(P-P)FeH]⁺ to acridine radicals, the bulkier acridinium salt 9-phenyl-10-methylacridinium (PhAcr⁺) was selected as an acceptor. More evidence for this “two-step (e⁻/H[•])” process was derived from the characterization of PhAcr[•] and [4H]⁺ radicals by EPR spectra and by the crystallographic structure confirmation of [4H]⁺. Our mechanistic understanding of fundamental H⁻ transfer from iron(II) hydrides to NAD⁺ analogues provides insight into establishing attractive bio-organometallic transformation cycles driven by iron catalysis.

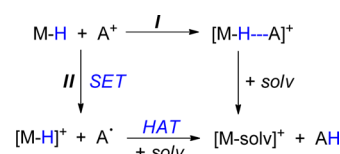


INTRODUCTION

So-called “organo-hydrides”,¹ or nicotinamide cofactor NAD(P)H analogues such as dihydronicotinamides and 1,4-dihydropyridines,^{2,3} are widely used as reducing agents in hydrogenation and transfer hydrogenation catalysis.^{4–6} Regeneration of NAD⁺/NADH model compounds by metal catalysis is significant in the establishment of transformation cycles.^{7–10} In this context, hydride (H⁻) transfer from metal hydrides M–H to pyridinium, iminium, acridinium, and other organic cation salts is a ubiquitous elemental step and a knowledge of M–H cleavage^{11–13} during H⁻ transfer is essential, because it provides a qualitative strategy for catalyst design.

In principle, there are two pathways for H⁻ transfer in the reported reactions of M–H and organo-cations A⁺, as shown in Scheme 1. These are the “single-step H⁻” transfer path (I) and the “two-step (e⁻/H[•])” path (II).¹⁴ Transfer of a hydride (H⁻) is usually achieved via nucleophilic attack on organo-cations. Twenty years ago, Hembre et al. reported H⁻ transfer from Cp*(dppm)RuH (Cp* = C₅Me₅⁻, dppm = Ph₂PCH₂PPh₂) to *N*-methylquinolinium salts.¹⁰ The presence of an electron-transfer inhibitor, [MV]²⁺ (MV = methyl viologen), had no effect on methylquinolinium reduction, thus excluding an H⁻ transfer process initiated by an ET step. Norton et al. investigated the reduction of iminium cations to imines by

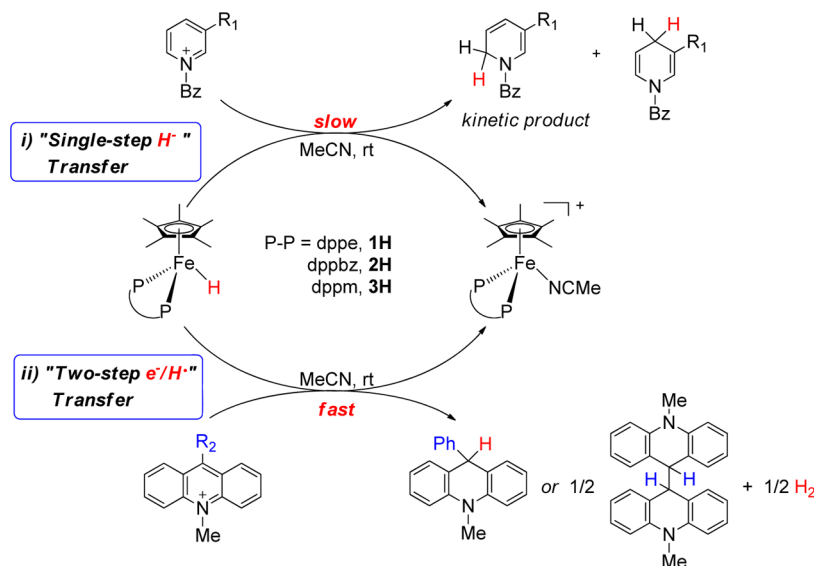
Scheme 1. Two Pathways of H⁻ Transfer from M–H to Organic Cation Acceptors (A⁺)^a



^aAbbreviations: SET, single-electron transfer; HAT, hydrogen atom transfer; solv, coordinating solvent molecules such as MeCN and H₂O.

Cp'(P-P)RuH hydrides (Cp' = C₅H₅⁻ or C₅Me₅⁻ anion, P-P = chelating diphosphine)¹⁶ and reported that the H⁻ transfer reaction is significantly affected by the electronic and steric properties of the chelating diphosphine ligand on the Ru(II) center. When 1-benzylpyridinium cation (BNA⁺), resembling oxidized NAD⁺ cofactor, is used as an H⁻ acceptor, it gives mainly the reduction product, 1-benzyl-dihydronicotinamide (BNAH), as the two isomers 1,6- and 1,4-BNAH. Fish et al. reported H⁻ transfer from [Cp*(bpy)RhH]⁺ (bpy = 2,2'-bipyridine) to BNA⁺, producing 1,4-BNAH as the kinetic

Received: March 2, 2016

Scheme 2. H⁻ Transfer from Cp*(P-P)FeH to *N*-Benzylpyridinium and Acridinium Salts

product.¹⁷ Regioselective production of 1,4-BNAH was thought to be through a transition state in which the oxygen atom of the carbamoyl group in BNA⁺ was coordinated to the metal center and the Cp* ring changed its coordination mode from η^5 to η^3 . This transition state could cause the C4 position to be more electrophilic toward attack. Ishitani et al. reported the interactions between [(tpy)(bpy)RuH]⁺ (tpy = 2,2':6'2''-terpyridine) and BNA⁺ salts, forming a [Ru-BNAH]⁺ adduct.¹⁸ However, such interactions have also been observed in NMR studies,¹⁹ even in pyridinium salts with a noncoordinating group at the C3 position. A two-step (e⁻/H[•]) pathway is more likely to operate in cases in which the M–H and organo-cations have close redox potentials. Norton et al. reported that reduction of acylpyridinium salts by Cp*Ru(dppf)H (dppf = 1,1'-bis(diphenylphosphino)ferrocene) is initiated by a “single-electron-transfer” (SET) step, followed by a hydrogen atom transfer (HAT) step.¹⁴

Although hydrides (M–H) based on noble metals (M = Ru,^{14–16,18–20} Ir,²¹ Rh^{17,22}) have been well investigated in this field, studies based on abundant metal hydrides are sparse. In recent years, remarkable progress has been made in hydrogenation and transfer hydrogenation catalysis by first- and second-row metals.^{23,24} We have been interested in the reduction of NAD⁺ cation models by using hydrido iron(II) complexes, and previous work with Rauchfuss et al. has demonstrated the hydridic character of a diiron dihydride compound toward benzimidazolium salts.²⁵

In this paper, we examine the role of the well-known iron(II) hydride complexes of the “piano-stool” type, Cp*(P-P)FeH (P-P = chelating diphosphine), in the reduction of *N*-benzylpyridinium and acridinium salts. Significantly, two different mechanisms were found in the process of H⁻ transfer from Cp*(P-P)FeH to these organo-cations (Scheme 2): a single-step H⁻ transfer to pyridinium and a two-step (e⁻/H[•]) transfer for acridinium reduction.

RESULTS AND DISCUSSION

Synthesis and Characterization. The compound Cp*(dppe)FeH²⁶ (dppe = 1,2-C₂H₄(PPh₂)₂; **1H**) and its new analogues Cp*(dppbz)FeH (dppbz = 1,2-C₆H₄(PPh₂)₂; **2H**), Cp*(dppm)FeH (dppm = Ph₂PCH₂PPh₂; **3H**),

and Cp*(dcpe)FeH (dcpe = 1,2-C₂H₄(PCy₂)₂; **4H**) were synthesized in good yields using modified published methods. FeCl₂ was added to 1 equiv of Cp*Li in THF, and the mixture was stirred at room temperature for 1 h. Two equiv amount of KPF₆ in MeCN was added to give [Cp*Fe(NCMe)₃]PF₆, which was precipitated by diethyl ether as a deep purple solid. This precursor was used to prepare various [Cp*(P-P)Fe(NCMe)]⁺ salts by adding the corresponding diphosphine. The MeCN ligand in [Cp*(P-P)Fe(NCMe)]⁺ was displaced by a hydride from Bu₄NBH₄ to give Cp*(P-P)FeH compounds. The ¹H NMR spectra of **1H** and **2H** exhibit hydride resonances at around δ –16 (t, J_{P-H} = 69 Hz), and the ³¹P NMR spectra display a singlet at δ 107.8 for **1H** and at δ 102.6 for **2H**. In comparison with **1H** and **2H**, the hydride signal shifts to δ –11.9 in **3H** and δ –17.4 in **4H**.

All of the synthesized complexes of [Cp*(P-P)Fe(NCMe)]⁺ and Cp*(P-P)FeH were structurally characterized by crystallographic analysis. The structures of **2H**–**4H** are depicted in Figure 1, and other structures are shown in Figures S1–S5 in the Supporting Information. A comparison of P–Fe–P bite angles among these iron(II) complexes is provided in Table 1. The bite angle in Cp*(P-P)FeH is larger than those in the corresponding parent [Cp*(P-P)Fe(NCMe)]⁺ cations. The bite angles (\angle P–Fe–P) in **1H** and **2H** differ by only ca. 0.2°. Such minor differences of binding effects between dppe and dppbz have also been observed in Cp*(P-P)RuH compounds.¹⁶ In comparison to dppbz, the more bulky dcpe group increases the bite angle in **4H** by about 1.4°, while the dppm ligand experiences steric constriction at the Fe center in **3H** with its bite angle of 75.33(4)°.

Single-Step H⁻ Transfer to BNA⁺. Stoichiometric reactions between Cp*(P-P)FeH (**1H** or **2H**) and BNA⁺ were conducted in a J. Young tube in CD₂Cl₂/CD₃CN (v/v 2/1) at room temperature. Analysis of the ¹H NMR spectra suggests that BNA⁺ was reduced quantitatively to give 1,4-BNAH (yield >90%) and 1,6-BNAH (yield <10%) overnight (eq 1). ³¹P NMR spectroscopic studies confirm that the organoiron product was exclusively composed of [Cp*(P-P)Fe(NCMe)]⁺ cations. Interestingly, there no reaction was observed in THF.

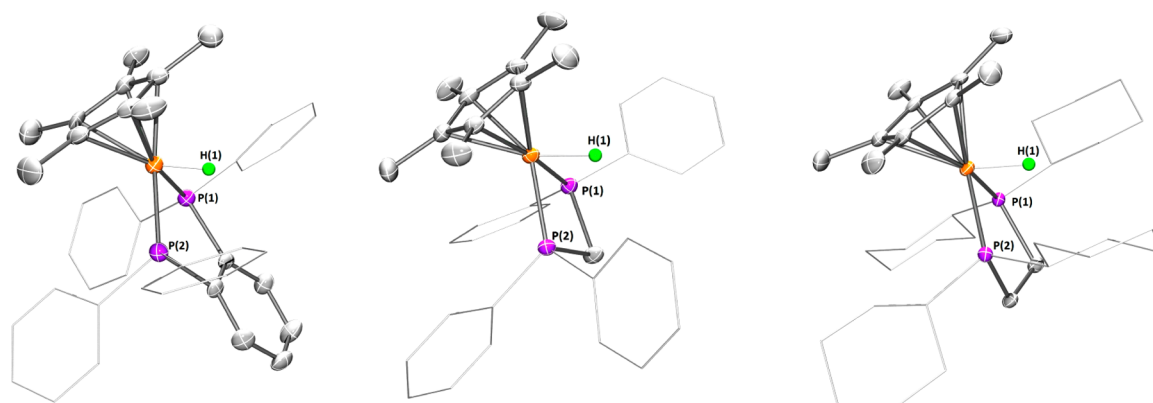
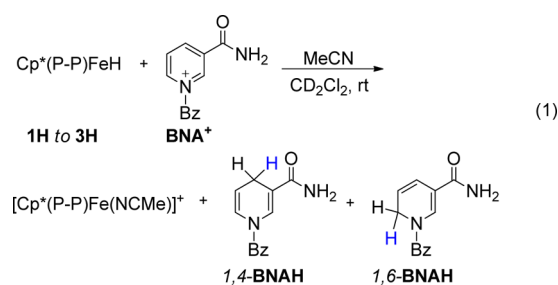


Figure 1. Structures (50% probability thermal ellipsoids) of **2H** (left), **3H** (center), and **4H** (right). For clarity, the four phenyl groups bound to phosphorus are drawn as lines and hydrogen atoms are omitted. Selected distances (Å) and angles (deg): **2H**, Fe–P(1) 2.1368(8), Fe–P(2) 2.1289(8), P(1)–Fe–P(2) 85.99(3); **3H**, Fe–P(1) 2.1479(10), Fe–P(2) 2.1531(10), P(1)–Fe–P(2) 75.33(4); **4H**, Fe–P(1) 2.1712(7), Fe–P(2) 2.1855(7), P(1)–Fe–P(2) 87.44(3).

Table 1. NMR Spectroscopic Properties and Bite Angles of P–Fe–P in Iron Complexes

complex	ligand	$\delta(^1\text{H}, \text{Fe-H})$ ($J_{\text{P-H}}$, Hz)	$\delta(^{31}\text{P})$	$\angle\text{P-Fe-P}$ (deg) (vs $[\text{Cp}^*(\text{P-P})\text{Fe}(\text{NCMe})]^+$) ^a
1H	dppe	−16.7 (t, 69)	107.8	86.22(7) (85.48(7))
2H	dppbz	−16.1 (t, 69)	102.6	85.99(3) (83.90(4))
3H	dppm	−11.9 (td, 63)	45.9	75.33(4) (74.47(4))
4H	dcpe	−17.4 (t, 72)	113.7	87.44(3) (85.36(4))

^aComparison of the bite angle of P–Fe–P with that of the corresponding $[\text{Cp}^*(\text{P-P})\text{Fe}(\text{NCMe})]^+$ cation.



In order to gain insight into the possible mechanistic steps of 1,4-BNAH (major) and 1,6-BNAH (minor) formation, we followed the kinetics for reactions of $\text{Cp}^*(\text{P-P})\text{FeH}$ with 10 equiv of BNA^+ at various concentrations by ^1H NMR spectroscopy. For **2H**, the concentrations $[\text{1,4-BNAH}]$, $[\text{1,6-BNAH}]$, and $[\text{BNAH}]$ observed over time are shown in Figure 2. During the H^- transfer reaction, both $[\text{1,4-BNAH}]$ and $[\text{1,6-BNAH}]$ increased slowly and, after the amount of reduced BNAH reached a plateau, the isomerization process of 1,6-BNAH to 1,4-BNAH continued. The results suggest that the 1,4-product is more thermally stable^{2a,27} and the kinetic production of 1,6-BNAH was clearly demonstrated for **2H**. For the production of BNAH, a pseudo-first-order rate constant (k_{obs}) can be linearly correlated with $[\text{BNA}^+]$. The rate constant of H^- transfer of BNAH reduction for **2H** is $4.45 \times 10^{-3} \text{ M}^{-1} \text{ s}^{-1}$, which is comparable to $3.23 \times 10^{-3} \text{ M}^{-1} \text{ s}^{-1}$ for **1H** (Figure S25 in the Supporting Information) at 298 K.

Surprisingly, the reaction of **3H** and BNA^+ was complete in 10 min at room temperature, and the yields of 1,6- and 1,4-BNAH were 36% and 64%, respectively. The H^- transfer process was too fast to allow measurement of k_{obs} under pseudo-first-order conditions. The rate constant was measured using a **3H**/ BNA^+ ratio of 1/2. Under these conditions, a second-order reaction would follow the equation shown in Figure 3.^{16a,22b} The plot of the result confirms a linear

relationship between $\ln\{1 + [\text{3H}]_0/[\text{3H}]_t\}$ and t , and the y intercept (0.746) is consistent with $\ln 2$. The rate constant k for H^- transfer from **3H** to BNA^+ derived from the slope is $1.74 \times 10^{-1} \text{ M}^{-1} \text{ s}^{-1}$, which is nearly 40 times that for **2H** ($k = 4.45 \times 10^{-3} \text{ M}^{-1} \text{ s}^{-1}$). This is mainly due to a 10.7° smaller bite angle ($\angle\text{P-Fe-P}$) in **3H** than in **2H**. The significance of the bite angle effect on H^- transfer rates was also found in the case of $\text{CpRu}(\text{dppm})\text{H}$ and an iminium cation.^{16a}

To explore whether substituents (R) at the C3 position affect H^- transfer, a broad class of pyridinium cations were investigated as hydride acceptors of **2H**. Table 2 shows the results for the reactions between **2H** and various BNA^+ cation analogues under the same conditions. *N*-Benzylpyridinium salts with a $-\text{CONEt}_2$ substituent at the C3 position decreased the hydride transfer rate considerably. Only 65% conversion was achieved in 7 days, which suggests that the H^- transfer reaction is affected by steric factors in the substrates. An electronic effect also plays an important role in this reaction. Generally, electron-withdrawing groups such as $-\text{COCH}_3$, $-\text{COOCH}_3$, and $-\text{CF}_3$ accelerate H^- transfer, while electron-donating groups (e.g. $-\text{CH}_3$) have the opposite effect.

In the most of these H^- transfer reactions, *N*-benzyl-1,4-dihydropyridine derivatives were observed as the major product. However, the thermodynamic stability of the 1,6-product seems very dependent on an electron-withdrawing group at C3. For $-\text{COOCH}_3$ and $-\text{CF}_3$ groups (Table 2, entries d and e), 1,6-products remain dominant after 10 h of reaction. A slow conversion of 1,6-BzPyH- CF_3 to 1,4-BzPyH- CF_3 was observed, as shown in Figure 4, from the kinetics of the reaction between **2H** and BzPy-CF_3^+ .

With the exception of the *N*-benzyl-3-CN-pyridinium salt (BzPy-CN^+), containing a $-\text{CN}$ group at C3, there was no interaction observed between the pyridinium salts and $\text{Cp}^*(\text{P-P})\text{FeH}$. For the reaction of BzPy-CN^+ with **2H**, the ^{31}P NMR spectrum displays not only a singlet at δ 96.2 for

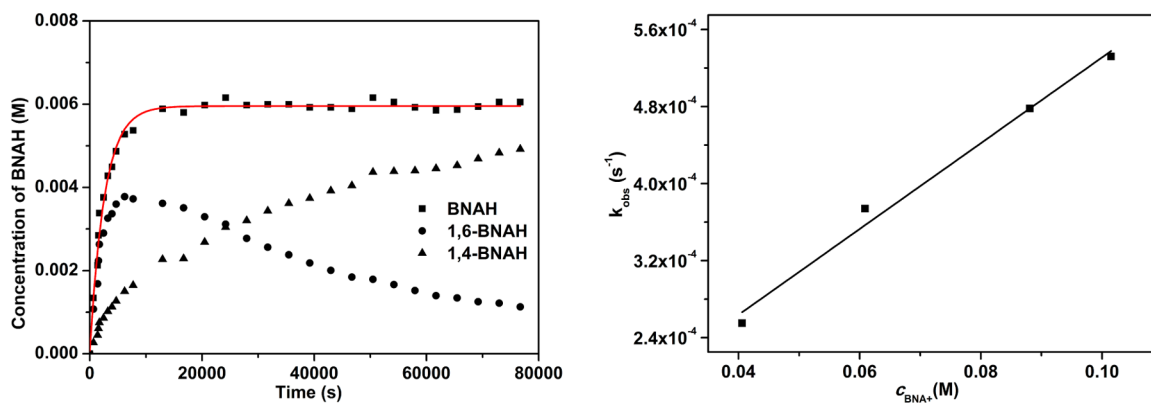


Figure 2. (left) Concentrations of BNAH, 1,4-BNAH, and 1,6-BNAH over time detected in the reaction of **2H** and BNA⁺ in CD₂Cl₂/CD₃CN (2/1) at 298 K. The initial [**2H**] and [BNA⁺] are 6.09 × 10⁻³ M and 6.09 × 10⁻² M, respectively. (right) Plot of k_{obs} vs [BNA⁺] for the reaction of **2H** and BNA⁺. Results: $k = 4.45 \times 10^{-3} \text{ M}^{-1} \text{ s}^{-1}$, $R^2 = 0.9847$.

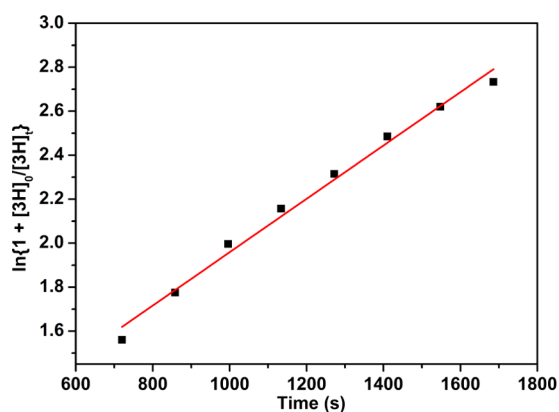


Figure 3. Plot of $\ln\{1 + [3\text{H}]_t/[3\text{H}]_0\}$ vs time (t) for hydride transfer from **3H** to BNA⁺ in CD₂Cl₂/CD₃CN (2/1) at 298 K. Rate equation: $\ln\{1 + [3\text{H}]_t/[3\text{H}]_0\} = \ln 2 + k[3\text{H}]_0 t$, where [BNA⁺]₀ and [3H]₀ are the initial concentrations of BNA⁺ (1.39 × 10⁻² M) and **3H** (6.95 × 10⁻³ M), [3H]_t is the concentration of **3H** at time t , and k is the second-order rate constant. Results: $k = 1.74 \times 10^{-1} \text{ M}^{-1} \text{ s}^{-1}$, $R^2 = 0.9886$.

Table 2. Pseudo-First-Order Rates of Hydride Transfer from **2H to BNA⁺ Cation Analogues at 298 K**

entry	R ^a	conversion ^b (%)	ratio (1,6/1,4 isomer)	k_{obs} ^c (s ⁻¹)
a	-CONH ₂	100	24/76	4.78 × 10 ⁻⁴
b	-CONEt ₂	62 ^d	9/53	very slow ^d
c	-COCH ₃	100	20/80	2.64 × 10 ⁻³
d	-COOCH ₃	100	57/43	3.27 × 10 ⁻³
e	-CF ₃	100	91/9	3.76 × 10 ⁻³
f	-CH ₃	NR ^e		
g	-H	100	7/93	3.92 × 10 ⁻⁴

^aR is the substituent on C3 of *N*-benzylpyridinium. ^bThe conversions and ratios of products were determined by ¹H NMR analysis after 12 h of reaction. Initial concentrations of **2H** and BNA⁺ analogues were the same at 8.81 × 10⁻³ M. ^cThe k_{obs} values were determined under pseudo-first-order conditions. Initial concentrations of **2H** and BNA⁺ analogues were 8.81 × 10⁻³ and 8.81 × 10⁻² M, respectively. ^d168 h. ^eNo reaction was observed in 72 h.

[**2**(NCMe)]⁺ but also a new singlet at δ 92. These new products were thought to be [BzPyH-CN-**2**]⁺ according to the ESI-MS spectral analysis, which showed an ion peak at m/z 833.3255 corresponding to [**2** + BzPyH-CN]⁺. However, the

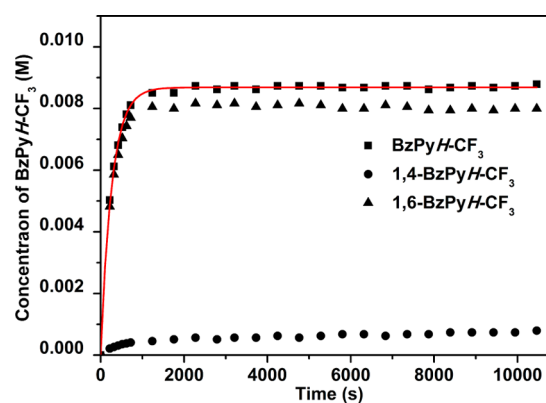


Figure 4. Concentrations of BzPyH-CF₃, 1,4-BzPyH-CF₃ and 1,6-BzPyH-CF₃ over time detected for the reaction of **2H** and BzPyH-CF₃⁺ in CD₂Cl₂/CD₃CN (2:1) at 298 K. The initial [**2H**] and [BzPyH-CF₃⁺] are 8.81 × 10⁻³ and 8.81 × 10⁻² M, respectively.

¹H NMR spectrum of the reaction mixture displayed proton signals not only at the C4 position for [1,4-BzPyH-CN-**2**]⁺ (δ 2.40) but also for free 1,4-BzPyH-CN (δ 3.09) and proton signals on the C6 position for [1,6-BzPyH-CN-**2**]⁺ (δ 3.91) and free 1,6-BzPyH-CN (δ 4.01). These results suggest that [1,4-BzPyH-CN-**2**]⁺ and [1,6-BzPyH-CN-**2**]⁺ exhibit the same phosphorus nuclear magnetic resonance.

We next examined the use of **1H** as an H⁻ donor for BzPy-CN⁺. The ³¹P NMR spectrum displays a singlet at δ 90.2 for [1(NCMe)]⁺ and also a new singlet at δ 89.7. Fortunately, [1,4-BzPyH-CN-**1**]⁺ from the reaction could be crystallographically characterized (Figure 5). In this new complex, reduced *N*-benzyl-1,4-dihydropyridine-3-carbonitrile (1,4-BzPyH-CN) was coordinated to the iron center of **1**⁺.

We found that both 1,4-BzPyH-CN and BzPy-CN⁺ replaced the MeCN ligand in [Cp*(P-P)Fe(NCMe)]⁺, giving [Cp*Fe(P-P)(1,4-BzPyH-CN)]⁺ and [Cp*Fe(P-P)(BzPy-CN)]²⁺ complexes with the crystal structures shown in Figure 5. Furthermore, [Cp*Fe(P-P)(1,4-BzPyH-CN)]⁺ released 1,4-BzPyH-CN in MeCN to afford [Cp*(P-P)Fe(NCMe)]⁺, and finally an reaction equilibrium was observed, judging from NMR spectral studies (Figures S44–S47 in the Supporting Information). Though a H⁻ transfer mechanism based on coordination or interaction between pyridinium salts to Ru and Rh hydride complexes was considered,^{17–19} the

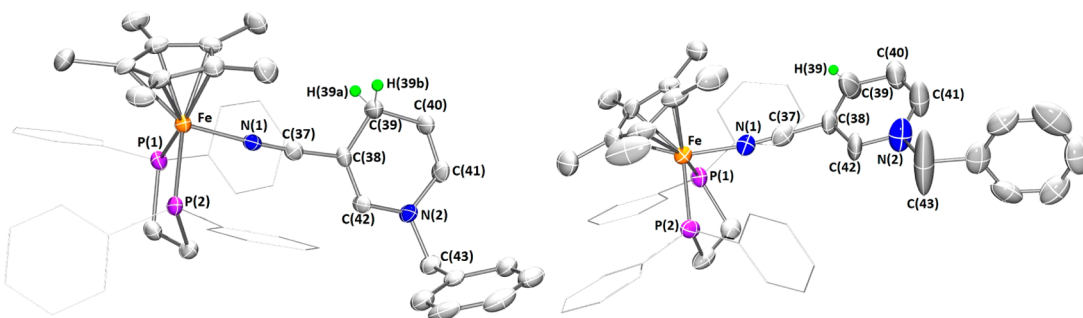
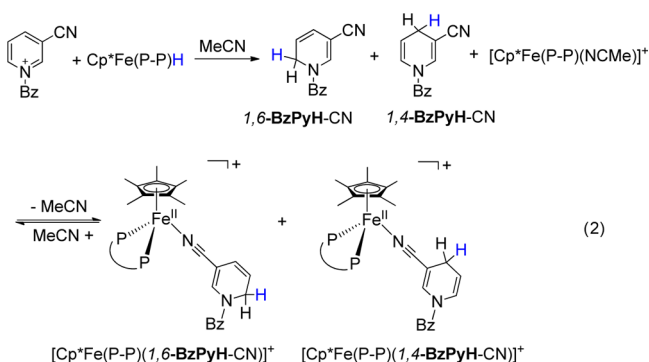


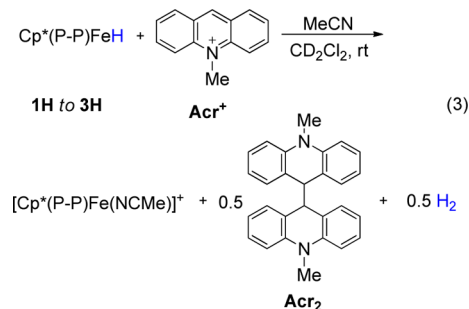
Figure 5. Structures (50% probability thermal ellipsoids) of [1,4-BzPyH-CN-1]⁺ (left) and [BzPy-CN-1]²⁺ (right) cations. For clarity, the PF₆[−] counteranions are not shown, the four phenyl groups bonded to phosphorus are drawn as lines, and hydrogen atoms are omitted. Selected distances (Å) and angles (deg): [1,4-BzPyH-CN-1]⁺, Fe–P(1) 2.2505(19), Fe–P(2) 2.2155(18), Fe–N(1) 1.888(5), N(1)–C(37) 1.154(7), C(37)–C(38) 1.414(8), C(38)–C(39) 1.513(8), C(38)–C(42) 1.329(8), C(41)–N(2) 1.411(7), N(2)–C(42) 1.363(7), P(1)–Fe–P(2) 85.38(6); [BzPy-CN-1]²⁺, Fe–P(1) 2.223(3), Fe–P(2) 2.232(3), Fe–N(1) 1.872(9), N(1)–C(37) 1.133(12), C(37)–C(38) 1.432(15), C(38)–C(39) 1.440(17), C(38)–C(42) 1.350(15), C(41)–N(2) 1.372(16), N(2)–C(42) 1.351(13), P(1)–Fe–P(2) 85.77(11).



reaction path depicted in eq 2 cannot be excluded for BzPy-CN⁺ and Cp*(P-P)FeH.

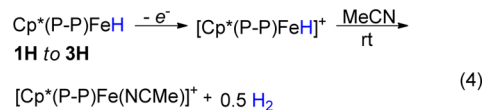
Our studies indicate that the reactions between Cp*(P-P)FeH and BNA⁺ proceed by a single-step H[−] transfer pathway, in which the hydride ligand as a nucleophile attacks the C6 position in the BNA⁺ cation, affording 1,6-BNAH as a kinetic product. The steric factor arising from the diphosphine chelating ligand affects the reaction rates significantly. The transfer of H[−] to BNA⁺ analogues is more likely to be charge controlled,¹⁴ although steric factors also influence the rates. *N*-Benzylpyridinium cations with electron-withdrawing substituents at C3 favor the positive charge at C6, allowing nucleophilic attack by H[−], which is reflected in increased reaction rates.

Two-Step “e[−]/H[−]” Transfer to Acridinium Salts. When acridinium salts were used as the acceptors, the chemistry differs greatly from that described for *N*-benzylpyridinium salts. Treatment of the Cp*(P-P)FeH (**1H**–**3H**) with 10-methylacridinium (Acr⁺) salts in CD₂Cl₂/MeCN (v/v 100/1) led quantitatively to organoiron products of [Cp*(P-P)Fe(NCMe)]⁺, as indicated by ³¹P NMR analysis (eq 3). However, ¹H NMR spectra indicated



that no 10-methyl-9,10-dihydroacridine was produced. Furthermore, the hydrido iron(II) complexes were found to react readily with Acr⁺ with evolution of H₂. The yield of H₂, quantified by GC analysis, was 43% (three experiments, standard deviation of 3%) relative to the amounts of Cp*(P-P)FeH (**1H**–**3H**). The organic product isolated from the reactions was identified as the Acr₂ dimer by ¹H NMR analysis. The structure of the Acr₂ dimer was confirmed crystallographically, in which the two Acr planes enjoy parallel head-to-head bonding by C9–C9' (Figure S52 in the Supporting Information). Apparently, there is an electron transfer from iron(II) hydrides to Acr⁺ with generation of an Acr[•] radical, which produces Acr₂ dimer.

Oxidation of Cp*(P-P)FeH (**1H**–**3H**) by Acr⁺ salts in principle gives the [Cp*(P-P)FeH]⁺ radical. Tilset et al. reported that oxidation of group 6 cyclopentadienyl metal hydrides leads to the corresponding hydride cation radicals, which are more acidic than their neutral parent by a relatively constant 20.6 ± 1.5 pK_a units.²⁸ Most of the 17-electron cationic hydride radicals are short-lived and undergo deprotonation,²⁹ disproportionation, and H₂ elimination.^{30,31} Though [**1H**]⁺ has been isolated at −60 °C in CH₂Cl₂,³² we found that oxidation of **1H** (or **2H**, **3H**) by [FeCp₂]BF₄ in CH₂Cl₂/MeCN (v/v 100/1) at room temperature resulted in release of H₂ and formation of [Cp*(P-P)Fe(NCMe)]⁺, as shown in eq 4.



To confirm the [Cp*(P-P)FeH]⁺ radical postulated as an intermediate resulting from ET of iron hydride to Acr⁺, **4H** was selected as a hydride donor. The bulkier and more electron rich dcp e ligand [**4H**]⁺ was expected to be stable at room temperature and to allow further characterization. After the reaction of **4H** and Acr⁺, the solvent was removed under vacuum (eq 5). The Acr₂ was isolated by washing the residue with toluene. The organoiron complex in the residue was redissolved in CH₂Cl₂ and crystallized by allowing a hexane layer to diffuse into the CH₂Cl₂ solution.

Crystallographic analysis reveals an ionic complex of the type [Cp*(P-P)FeX]PF₆ (Figure 6). This framework is similar to that of the neutral hydride of **4H**. The bite angle of P–Fe–P in **4H**⁺ is 89.172(19)°, 1.7° larger than that of **4H**. The hydride

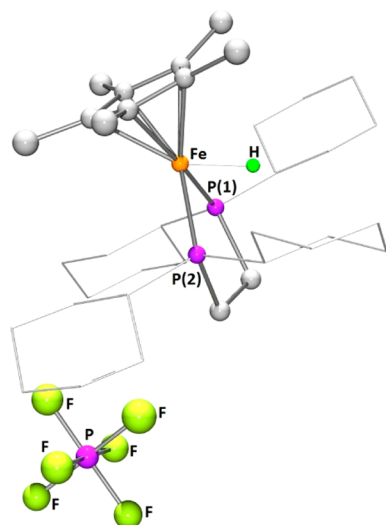
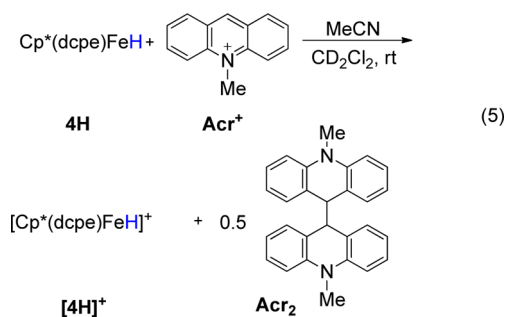


Figure 6. Structure (50% probability thermal ellipsoids) of $[\text{4H}]\text{PF}_6$ salts. For clarity, four phenyl groups bound to phosphorus are drawn as lines and hydrogen atoms are omitted. Selected distances (Å) and angles (deg): Fe–P(1) 2.2481(5), Fe–P(2) 2.2561(5), P(1)–Fe–P(2) 89.172(19).

ligand was located in a different map, and its position and isotropic displacement parameters were refined. Reduction of $[\text{4H}]\text{PF}_6$ by 1 equiv of Cp_2Co in THF afforded 4H , as indicated by ^1H and ^{31}P NMR analysis. These results prove that the hydride ligand persists in the chemical redox reaction of $\text{4H}/\text{4H}^+$.

More evidence of 4H^+ formation was derived from EPR studies (Figure 7). The X-band EPR spectrum of 4H^+ , recorded at 90 K

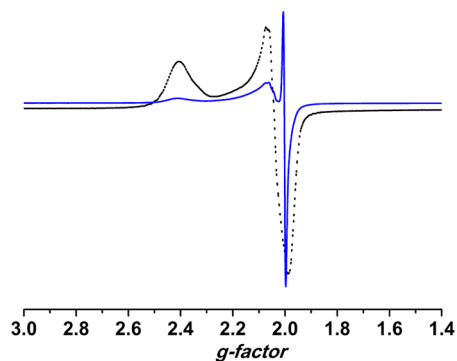


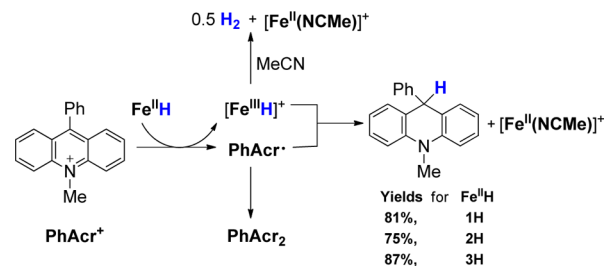
Figure 7. X-band EPR spectra of $[\text{4H}]\text{PF}_6$ (black dotted line) and reaction of 4H with PhAcr^+ (blue line) recorded in THF at 90 K.

in THF, exhibits three well-separated signals corresponding to the three g tensor components ($g_1 = 1.980$, $g_2 = 2.036$, $g_3 = 2.395$),

values that contrast with those determined for the 17-electron 1H^+ ($g_1 = 1.9944$, $g_2 = 2.0430$, $g_3 = 2.4487$).^{32,33} The initial ET step from 4H to Acr^+ generates 4H^+ and Acr^\bullet radical species, and the latter is highly susceptible to dimerization. While using bulky 10-methyl-9-phenylacridinium (PhAcr^+), we expected that the phenyl substituent at the C9 position would stabilize PhAcr^\bullet in contrast to the Acr^\bullet radical. Indeed, the X-band EPR spectrum for the reaction mixture of 4H and PhAcr^+ clearly showed the formation of 4H^+ . The new sharp signal with a g value of 2.0029 is close to the free-electron g value of 2.0023, implying the formation of PhAcr^\bullet .

The reaction mixture of 4H and PhAcr^+ was always NMR silent at room temperature, probably because 4H^+ was too stable to donate the H^\bullet atom to PhAcr^\bullet after the initial ET process. To explore the second step of hydrogen atom transfer (HAT) from $[\text{Cp}^*(\text{P-P})\text{FeH}]^+$ to the PhAcr^\bullet radical, we examined the reaction of PhAcr^+ with 1H – 3H . PhAcrH was produced unambiguously in yields ranging from 75 to 87%, as shown in Scheme 3. A small amount of H_2 was also released

Scheme 3. Reactions Observed between PhAcr^+ and Iron Hydrides



(yield <10%), as shown by GC analysis, while the conversions of $\text{Cp}^*(\text{P-P})\text{FeH}$ and PhAcr^+ are nearly quantitative. The above results indicate that the second step of HAT from $[\text{Cp}^*(\text{P-P})\text{FeH}]^+$ to PhAcr^\bullet competes with PhAcr^\bullet dimerization and intermolecular H_2 evolution from $[\text{Cp}^*(\text{P-P})\text{FeH}]^+$ (Scheme 3).

To understand the plausible electron-transfer process, redox properties were evaluated for these iron(II) hydride compounds and NAD^+ cation analogues (Figure 8). Cyclic voltammograms of 1H – 4H in CH_2Cl_2 exhibit reversible redox events involving the $[\text{Fe}^{\text{II}}\text{H}]^0/[\text{Fe}^{\text{III}}\text{H}]^+$ couple. The oxidation potentials of 1H – 3H are all approximately -0.36 V, mainly due to the similar electron-donating abilities of dppe , dppbz , and dppm . With a more electron rich dcpe ligand, 4H was oxidized at the more negative potential of -0.44 V. The oxidation potentials of $\text{Cp}(\text{dppe})\text{RuH}$ and $\text{Cp}^*(\text{dppe})\text{-RuH}$ are -0.16 and -0.51 V,⁶ suggesting that $\text{Cp}^*(\text{P-P})\text{FeH}$ is more electron rich than $\text{Cp}(\text{dppe})\text{RuH}$ but less so than $\text{Cp}^*(\text{dppe})\text{RuH}$ hydrides. The reduction potentials of NAD^+ cation analogues are more negative than the potentials of $[\text{Cp}^*(\text{P-P})\text{FeH}]^{0/+}$ couples. BNA^+ exhibits an irreversible reduction event at -1.50 V in CH_2Cl_2 solution, while Acr^+ and PhAcr^+ salts have reduction potentials of -0.89 and -0.94 V, respectively.

According to the redox properties, the energy gap (ΔG_{ET}) of directly processing electron transfer from $\text{Cp}^*(\text{P-P})\text{FeH}$ to acridinium ranges from 0.48 to 0.58 eV, which is considerably smaller than the empirical critical limit of 1.0 eV for an endothermic ET process.³⁴ Such endergonic ET especially becomes possible when it is followed by rapid disproportionation

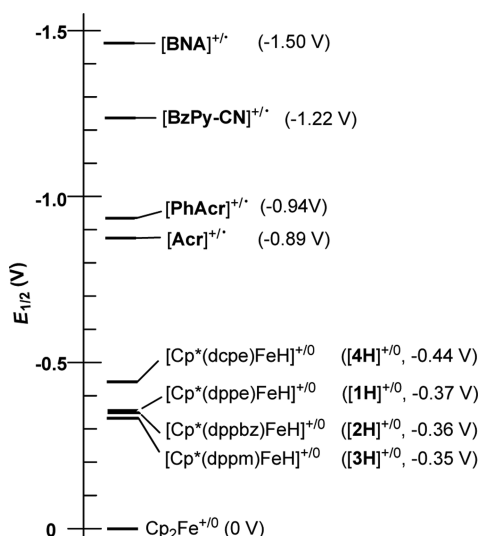


Figure 8. Redox potentials of $\text{Cp}^*(\text{P-P})\text{FeH}$ and NAD^+ cation analogues investigated.

reactions.³⁵ In our case, the subsequent highly exergonic processes are H_2 evolution, dimerization of Acrid^\bullet radicals, and HAT. These force the ET reduction of acridinium by $\text{Cp}^*(\text{P-P})\text{FeH}$ to go to completion.

CONCLUSIONS

In conclusion, we investigated the reactions between iron(II) hydride compounds of $\text{Cp}^*(\text{P-P})\text{FeH}$ and NAD^+ analogues. Unlike reported $\text{Ru}^{\text{II}}-\text{H}$ cases,^{18,19} there were no interactions between $\text{Fe}^{\text{II}}-\text{H}$ and BNA^+ analogues observed during H^- transfer reactions. Kinetics studies suggest that the BNA^+ model is reduced at the C6 position, affording 1,6-BNAH, which is converted to the more thermally stable 1,4-product. The reaction rate of this single-step H^- transfer process was highly improved by $\text{Cp}^*(\text{dppm})\text{FeH}$, with its less bulky diphosphine ligand. The results obtained from reduction of NAD^+ derivatives suggest that H^- transfer is more likely to be charge controlled. In the reduction of Acrid^+ , the reaction is initiated by an ET process that is then followed by rapid disproportionation reactions. To achieve HAT after ET, bulkier acridinium salts such as PhAcrid^+ should be used as acceptors. Thus, our current mechanistic understanding of fundamental H^- transfer from iron(II) hydride complexes to NAD^+ analogues provides valuable insight into establishing bio-organometallic transformation cycles driven by iron catalysis.

EXPERIMENTAL SECTION

Materials and Methods. All reagents were purchased from Sigma-Aldrich and used as received. All air-sensitive compounds were prepared and handled using standard Schlenk techniques or in a glovebox under an N_2 atmosphere. THF, pentane, and ether (dried by distillation over sodium) and CH_2Cl_2 and CH_3CN (dried by distillation over CaH_2) for general use were of AR grade and were stored under N_2 . CD_2Cl_2 , CD_3CN , C_6D_6 , and THF-d_8 were dried using molecular sieves (4 Å) and degassed by three thaw-freeze cycles. NMR spectra were recorded in J. Young NMR tubes on Bruker Avance 400 and Avance 300 spectrometers. ^1H NMR chemical shifts are referenced to the residual proton signal of the deuterated solvent. The ^{31}P NMR spectra were referenced to external H_3PO_4 . Single-crystal X-ray diffraction data were collected using a Bruker SMART APEX II diffractometer with a CCD area detector (graphite-monochromated $\text{Mo K}\alpha$ radiation) at 173 K. Infrared

spectra were obtained on a PerkinElmer FT-IR Spectrometer Spectrum Two in the range of $4000\text{--}450\text{ cm}^{-1}$ but are reported for the $\nu_{\text{Fe-H}}$ region only. Cyclic voltammetry was performed under nitrogen at room temperature using a CHI 760e electrochemical workstation (Shanghai Chen Hua Instrument Co., Ltd.) with a glassy-carbon working electrode, Pt-wire counter electrode, and an Ag-wire pseudoreference electrode.

BNA^+ salt substrates,³⁶ 10-methylacridinium iodide, and 9-phenyl-10-methylacridinium iodide³⁷ were synthesized according to published procedures. $\text{Cp}^*(\text{dippe})\text{FeH}^{26}$ and $[\text{Cp}^*\text{Fe}(\text{NCMe})_3]\text{PF}_6$ ³⁸ were synthesized in good yields by modified literature methods. Anion exchange reactions were conducted in water with saturated NH_4PF_6 aqueous solution.

Synthesis of $[\text{Cp}^*\text{Fe}(\text{NCMe})_3]\text{PF}_6$. $[\text{Cp}^*\text{Fe}(\text{NCMe})_3]\text{PF}_6$ was prepared by modification of the reported methods.³⁸ To a slurry of 850 mg (5.98 mmol) of Cp^*Li in 20 mL of THF was added 760 mg (5.98 mmol) of FeCl_2 , and the mixture was stirred for 1 h at room temperature. The solution gradually turned dark green. Then KPF_6 (1.10 g, 5.98 mmol) in 10 mL of CH_3CN was added. The solution turned deep purple within 5 min. Then the solvent was removed under vacuum and the residue was washed with Et_2O . The residue was recrystallized from $\text{CH}_3\text{CN}/\text{Et}_2\text{O}$, providing 2.19 g (80%) of $[\text{Cp}^*\text{Fe}(\text{NCMe})_3]\text{PF}_6$ as purple crystals. ^1H NMR (300 MHz, CD_3COCD_3): δ 2.42 (s, 9H, FeNCCH_3), 1.66 (s, 15H, Cp^*).

General Procedure for Preparation of $[\text{Cp}^*(\text{P-P})\text{Fe}(\text{NCMe})]\text{PF}_6$. To a purple solution of 230 mg (0.50 mmol) of $[\text{Cp}^*\text{Fe}(\text{NCMe})_3]\text{PF}_6$ in 40 mL of CH_3CN was added 1 equiv of the diphosphine ligand at room temperature. The mixture turned from purple to deep red immediately. After the solution was stirred for 3 h, the solvent was removed under vacuum and the residue was extracted with CH_2Cl_2 . Recrystallization from CH_2Cl_2 /pentane afforded red microcrystals.

$[\text{Cp}^*(\text{dppm})\text{Fe}(\text{NCMe})]\text{PF}_6$. Yield: 83%. ^1H NMR (300 MHz, CD_3CN): δ 7.44–7.59 (m, 20H, Ph), 4.58–4.71 (m, 1H, CH_2), 3.72–3.84 (m, 1H, CH_2), 1.96 (s, 3H, FeNCCH_3), 1.50 (s, 15H, Cp^*). ^{31}P NMR (121 MHz, CD_3CN): δ 34.8. ESI-MS: calcd for $[\text{Cp}^*\text{Fe}(\text{dppm})]^+$, 575.1720; found, 575.1837. Anal. Calcd for $\text{C}_{37}\text{H}_{40}\text{F}_6\text{FeNP}_3$: C, 58.33; H, 5.30; N, 1.84. Found: C, 57.82; H, 5.90; N, 1.55.

$[\text{Cp}^*(\text{dppbz})\text{Fe}(\text{NCMe})]\text{PF}_6$. Yield: 80%. ^1H NMR (400 MHz, CD_2Cl_2): δ 7.54–7.39 (m, 20H, Ph), 7.36–7.32 (m, 4H, Ph), 1.37 (s, 3H, FeNCCH_3), 1.31 (s, 15H, Cp^*). ^{31}P NMR (162 MHz, CD_2Cl_2): δ 96.2. ESI-MS: calcd for $[\text{Cp}^*\text{Fe}(\text{dppbz})]^+$, 637.1876; found, 637.1851. Anal. Calcd for $\text{C}_{42}\text{H}_{42}\text{F}_6\text{FeNP}_3$: C, 61.22; H, 5.14; N, 1.70. Found: C, 61.63; H, 5.32; N, 1.53.

$[\text{Cp}^*(\text{dcpe})\text{Fe}(\text{NCMe})]\text{PF}_6$. Yield: 82%. ^1H NMR (400 MHz, CD_3CN): δ 2.27 (t, 2H, CH_2), 2.20 (t, 2H, CH_2), 1.99 (s, 3H, FeNCH_3), 1.88–1.66 (m, 20H, C_6H_{20}), 1.59 (s, 15H, Cp^*), 1.50–1.30 (m, 24H, C_6H_{24}). ^{31}P NMR (162 MHz, CD_3CN): δ 83.9. ESI-MS: calcd for $[\text{Cp}^*\text{Fe}(\text{dcpe})]^+$, 613.3754; found, 613.3735. Anal. Calcd for $\text{C}_{38}\text{H}_{66}\text{F}_6\text{FeNP}_3$: C, 57.05; H, 8.32; N, 1.75. Found: C, 57.68; H, 8.56; N, 1.61.

General Procedure for Preparation of $\text{Cp}^*(\text{P-P})\text{FeH}$. To a THF solution of $[\text{Cp}^*(\text{P-P})\text{Fe}(\text{NCMe})]\text{PF}_6$ at $-30\text{ }^\circ\text{C}$ was slowly added 1 equiv of solid Bu_4NBH_4 . The temperature was increased to room temperature over a period of 3 h, and the solution turned orange. The solvent was removed under vacuum, leaving a gummy residue, which was extracted with pentane. The product was recrystallized from pentane and isolated by filtration.

$\text{Cp}^*(\text{dppm})\text{FeH}$. Yield: 70% of red solid. ^1H NMR (300 MHz, C_6D_6): δ 7.80–7.87 (m, 4H, Ph), 7.65–7.71 (m, 4H, Ph), 7.18–7.26 (m, 12H, Ph), 3.90–4.03 (m, 1H, CH_2), 3.30–3.40 (m, 1H, CH_2), 2.04 (s, 15 H, Cp^*), $-11.91(\text{td}, 1\text{H}, J_{\text{H-H}} = 6\text{ Hz}, J_{\text{P-H}} = 63.0\text{ Hz}, \text{Fe-H})$. ^{31}P NMR (162 MHz, C_6D_6): δ 45.9. Anal. Calcd for $\text{C}_{35}\text{H}_{38}\text{FeP}_2$: C, 72.89; H, 6.65. Found: C, 72.38; H, 6.35. IR (solid, $\nu_{\text{Fe-H}}$): 1827 cm^{-1} .

$\text{Cp}^*(\text{dppbz})\text{FeH}$. Yield: 80% of red solid. ^1H NMR (400 MHz, C_6D_6): δ 8.05 (t, 4H, Ph), 7.59 (t, 4H, Ph), 7.39–7.43 (m, 2H, Ph), 7.24–7.32 (m, 6H, Ph), 7.11–7.17 (m, 6H, Ph), 1.78 (s, 15H, Cp^*), -16.07 (t, 1H, $J_{\text{P-H}} = 69.0\text{ Hz}, \text{Fe-H})$. ^{31}P NMR (162 MHz,

C_6D_6): δ 102.6. Anal. Calcd for $C_{40}H_{40}FeP_2$: C, 75.21; H, 6.63. Found: C, 75.62; H, 6.52. IR (solid, ν_{Fe-H}): 1839, 1831 cm^{-1} .

$Cp^*(dcpe)FeH$. Yield: 75% of yellow solid. 1H NMR (400 MHz, C_6D_6): δ 2.05–1.89 (m, 16H, Cy), 2.13 (s, 15H, Cp*), 1.85–1.82 (t, 4H, CH_2), 1.49–1.29 (m, 24H, Cy), –17.4 (t, 1H, J_{P-H} = 73.1 Hz, Fe–H). ^{31}P NMR (162 MHz, C_6D_6): δ 113.7. Anal. Calcd for $C_{36}H_{64}FeP_2$: C, 41.82; H, 5.27. Found: C, 41.26; H, 5.54. IR (solid, ν_{Fe-H}): 1894 cm^{-1} .

Stoichiometric Hydride Transfer from $Cp^*(P-P)FeH$ to NAD^+ Analogues. In a typical experiment, $Cp^*(P-P)FeH$ and 1 equiv of the organic cation salts were placed in a vial in an N_2 -filled glovebox. A 0.5 mL portion of $CD_2Cl_2/MeCN$ (v/v 100/1) was added by gastight syringe, and the solution was transferred to a J. Young NMR tube before analysis by NMR.

$[Cp^*Fe(dppe)(1,4-BzPyH-CN)]PF_6$. To a solution of $Cp^*(dppe)FeH$ (40 mg, 0.066 mmol) in 2 mL of CH_2Cl_2 was added a solution of $[BzPy-CN]PF_6$ (22.5 mg, 0.066 mmol) in 3 mL of MeCN. After 1 h, the solvent was removed under vacuum. The residue was redissolved in CH_2Cl_2 , and crystals were grown by allowing a hexane layer to diffuse into the CH_2Cl_2 solution at -20 °C. 1H NMR (300 MHz, CD_2Cl_2): δ 7.58–7.35 (m, 23H, Ph), 7.19–7.16 (m, 2H, Ph), 5.65–5.62 (m, 1H, C6-H), 5.46 (s, 1H, C2-H), 4.62–4.60 (dt, 1H, C5-H), 4.13 (s, 2H, Ph CH_2), 2.55–2.54 (d, 2H, C4-H), 2.14–2.08 (m, 4H, CH_2), 1.31 (s, 15H, Cp*). ^{31}P NMR (162 MHz, CD_2Cl_2): δ 89.7. ESI-MS: calcd for $[Cp^*Fe(dppe)(1,4-BzPyH-CN)]^+$, 785.2877; found, 785.3177.

$[Cp^*Fe(dppbz)(1,4-BzPyH-CN)]PF_6$. 1H NMR (300 MHz, CD_2Cl_2): δ 7.43–7.00 (m, 29H, Ph), 5.54–5.49 (m, 1H, C6-H), 5.34 (s, 1H, C2-H), 4.48–4.43 (dt, 1H, C5-H), 4.00 (s, 2H, Ph CH_2), 2.32–2.31 (d, 2H, C4-H), 1.24 (s, 15H, Cp*). ^{31}P NMR (162 MHz, CD_2Cl_2): δ 92.3. ESI-MS: calcd for $[Cp^*Fe(dppbz)(1,4-BzPyH-CN)]^+$, 833.2877; found 833.3255.

$[Cp^*(dcpe)FeH]PF_6$. To a solution of $Cp^*(dcpe)FeH$ (30.7 mg, 0.05 mmol) in 2 mL of THF was added dropwise 3 mL of a THF solution of $AcrPF_6$ (17 mg, 0.05 mmol). After 5 min, the solvent was removed under vacuum. The residue was washed by toluene to remove Acr_2 . The organoiron complex in the residue was redissolved in CH_2Cl_2 and crystallized by allowing a hexane layer to diffuse into the CH_2Cl_2 solution. IR (solid, ν_{Fe-H}): 1934 cm^{-1} .

NMR Measurements of Rate Constants for Hydride Transfer from $Cp^*(P-P)FeH$ to NAD^+ Analogues. In a typical experiment, **1H** (4 mg, 0.0066 mmol) and $[BNA]PF_6$ (23.7 mg, 0.066 mmol) were placed in a vial under a nitrogen atmosphere in a glovebox. CD_2Cl_2 (0.5 mL) and CD_3CN (0.25 mL) were added by gastight syringe, and the solution was immediately transferred to a J. Young NMR tube. The first 1H NMR spectrum was recorded within 5 min, and then single-pulse spectra were taken every 300 s until the completion of the reaction. The integral values of the CH_2 of the benzyl group corresponding to 1,4-BNAH (4.21 ppm) and 1,6-BNAH (4.14 ppm) were compared to that of residual diethyl ether (m, 3.317–3.386 ppm).

EPR Experiments. EPR samples were prepared in a glovebox. The sample concentration was approximately 2 mM in THF. EPR spectra were recorded by using a Bruker ESP-300E spectrometer at 9.8 GHz, X-band, with 100 Hz field modulation.

H_2 Quantification by GC. The amount of evolved H_2 was quantified by a Techcomp 7890 II gas chromatograph (GC) equipped with a 5 Å molecular sieve column using argon as the carrier gas and a thermal conductivity detector. In a typical experiment, a Pyrex tube was filled with **2H** (4 mg, 0.0061 mmol) and Acr^+ (2.08 mg, 0.0061 mmol) in a glovebox. The tube was closed with a rubber plug and sealed with wax. Subsequently, 1 mL of CH_2Cl_2/CH_3CN (v/v 100/1) was injected into the tube. After the mixture was stirred for 10 min, CH_4 (200 μ L) was injected into the tube as an internal standard. A 200 μ L portion of the gas in the headspace was sampled by a Hamilton (1750 SL) gastight microliter syringe and then analyzed by GC. The amount of H_2 was calculated according to published methods.²⁵

■ ASSOCIATED CONTENT

Supporting Information

The Supporting Information is available free of charge on the ACS Publications website at DOI: 10.1021/acs.organomet.6b00179.

Experimental details, X-ray structures, NMR (1H , ^{31}P) spectra, and kinetics data (PDF)
X-ray crystallographic data (CIF)

■ AUTHOR INFORMATION

Corresponding Author

*E-mail for W.W.: wwg@sdu.edu.cn.

Notes

The authors declare no competing financial interest.

■ ACKNOWLEDGMENTS

We gratefully acknowledge the Natural Science Foundation of China and Shandong Province (21402107, 91427303 ZR2014BM011), fundamental research and subject construction funds, and the Young Scholars Program of Shandong University (2015WLJH23). We also thank Prof. Di Sun for assistance with the X-ray crystallography and Dr. Xuewang Gao for EPR experiments.

■ REFERENCES

- (1) (a) McSkimming, A.; Colbran, S. B. *Chem. Soc. Rev.* **2013**, *42*, 5439. (b) Zhu, X.-Q.; Zhang, M.-T.; Yu, A.; Wang, C.-H.; Cheng, J.-P. *J. Am. Chem. Soc.* **2008**, *130*, 2501. (c) Richter, D.; Mayr, H. *Angew. Chem., Int. Ed.* **2009**, *48*, 1958.
- (2) (a) Paul, C. E.; Arends, I. W. C. E.; Hollmann, F. *ACS Catal.* **2014**, *4*, 788. (b) Murakami, Y.; Kikuchi, J.; Hisaeda, Y.; Hayashida, O. *Chem. Rev.* **1996**, *96*, 721.
- (3) Eisner, U.; Kuthan, J. *Chem. Rev.* **1972**, *72*, 1.
- (4) Zheng, C.; You, S.-L. *Chem. Soc. Rev.* **2012**, *41*, 2498.
- (5) (a) Chen, Q.-A.; Chen, M.-W.; Yu, C.-B.; Shi, L.; Wang, D.-S.; Yang, Y.; Zhou, Y.-G. *J. Am. Chem. Soc.* **2011**, *133*, 16432. (b) Chen, Q.-A.; Gao, K.; Duan, Y.; Ye, Z.-S.; Shi, L.; Yang, Y.; Zhou, Y.-G. *J. Am. Chem. Soc.* **2012**, *134*, 2442.
- (6) Lu, L.-Q.; Li, Y.; Junge, K.; Beller, M. *Angew. Chem., Int. Ed.* **2013**, *52*, 8382.
- (7) (a) Quinto, T.; Köhler, V.; Ward, T. *Top. Catal.* **2014**, *57*, 321. (b) Abril, O.; Whitesides, G. M. *J. Am. Chem. Soc.* **1982**, *104*, 1552. (c) Wagenknecht, P. S.; Penney, J. M.; Hembre, R. T. *Organometallics* **2003**, *22*, 1180.
- (8) (a) Maenaka, Y.; Suenobu, T.; Fukuzumi, S. *J. Am. Chem. Soc.* **2012**, *134*, 367. (b) Fukuzumi, S.; Suenobu, T. *Dalton Trans.* **2013**, *42*, 18. (c) Maenaka, Y.; Suenobu, T.; Fukuzumi, S. *J. Am. Chem. Soc.* **2012**, *134*, 9417.
- (9) (a) Betanzos-Lara, S.; Liu, Z.; Habtemariam, A.; Pizarro, A. M.; Qamar, B.; Sadler, P. J. *Angew. Chem., Int. Ed.* **2012**, *51*, 3897. (b) Soldevila-Barreda, J. J.; Bruijninx, P. C. A.; Habtemariam, A.; Clarkson, G. J.; Deeth, R. J.; Sadler, P. J. *Organometallics* **2012**, *31*, 5958.
- (10) Hembre, R. T.; McQueen, S. *J. Am. Chem. Soc.* **1994**, *116*, 2141.
- (11) (a) Curtis, C. J.; Miedaner, A.; Ellis, W. W.; DuBois, D. L. *J. Am. Chem. Soc.* **2002**, *124*, 1918. (b) Tilset, M.; Fjeldahl, I.; Hamon, J.-R.; Hamon, P.; Toupet, L.; Saillard, J.-Y.; Costuas, K.; Haynes, A. *J. Am. Chem. Soc.* **2001**, *123*, 9984. (d) Cheng, T.-Y.; Bruntschwig, B. S.; Bullock, R. M. *J. Am. Chem. Soc.* **1998**, *120*, 13121.
- (12) (a) Morris, R. H. *J. Am. Chem. Soc.* **2014**, *136*, 1948. (b) *Recent Advances in Hydride Chemistry*; Peruzzini, M., Poli, R., Eds.; Elsevier: Amsterdam, 2001.
- (13) (a) Bourrez, M.; Steinmetz, R.; Ott, S.; Gloaguen, F.; Hammarström, L. *Nat. Chem.* **2015**, *7*, 140. (b) Matsubara, Y.; Fujita, E.; Doherty, M. D.; Muckerman, J. T.; Creutz, C. *J. Am. Chem. Soc.* **2012**, *134*, 15743.

- (14) Shaw, A. P.; Ryland, B. L.; Franklin, M. J.; Norton, J. R.; Chen, J. Y. C.; Hall, M. L. *J. Org. Chem.* **2008**, *73*, 9668.
- (15) Konno, H.; Sakamoto, K.; Ishitani, O. *Angew. Chem., Int. Ed.* **2000**, *39*, 4061.
- (16) (a) Guan, H.; Iimura, M.; Magee, M. P.; Norton, J. R.; Janak, K. E. *Organometallics* **2003**, *22*, 4084. (b) Guan, H.; Iimura, M.; Magee, M. P.; Norton, J. R.; Zhu, G. *J. Am. Chem. Soc.* **2005**, *127*, 7805.
- (17) (a) Lo, H. C.; Leiva, C.; Buriez, O.; Kerr, J. B.; Olmstead, M. M.; Fish, R. H. *Inorg. Chem.* **2001**, *40*, 6705. (b) Lo, H. C.; Buriez, O.; Kerr, J. B.; Fish, R. H. *Angew. Chem., Int. Ed.* **1999**, *38*, 1429.
- (18) (a) Matsubara, Y.; Koga, K.; Kobayashi, A.; Konno, H.; Sakamoto, K.; Morimoto, T.; Ishitani, O. *J. Am. Chem. Soc.* **2010**, *132*, 10547. (b) Kobayashi, A.; Konno, H.; Sakamoto, K.; Sekine, A.; Ohashi, Y.; Iida, M.; Ishitani, O. *Chem. - Eur. J.* **2005**, *11*, 4219. (c) Koga, K.; Matsubara, Y.; Kosaka, T.; Koike, K.; Morimoto, T.; Ishitani, O. *Organometallics* **2015**, *34*, 5530.
- (19) Matsubara, Y.; Kosaka, T.; Koga, K.; Nagasawa, A.; Kobayashi, A.; Konno, H.; Creutz, C.; Sakamoto, K.; Ishitani, O. *Organometallics* **2013**, *32*, 6162.
- (20) (a) Magee, M. P.; Norton, J. R. *J. Am. Chem. Soc.* **2001**, *123*, 1778. (b) Guan, H.; Saddoughi, S. A.; Shaw, A. P.; Norton, J. R. *Organometallics* **2005**, *24*, 6358. (c) Shaw, A. P.; Norton, J. R.; Buccella, D.; Sites, L. A.; Kleinbach, S. S.; Jarem, D. A.; Bocage, K. M.; Nataro, C. *Organometallics* **2009**, *28*, 3804.
- (21) (a) Hu, Y.; Li, L.; Shaw, A. P.; Norton, J. R.; Sattler, W.; Rong, Y. *Organometallics* **2012**, *31*, 5058. (b) Barrett, S. M.; Pitman, C. L.; Walden, A. G.; Miller, A. J. M. *J. Am. Chem. Soc.* **2014**, *136*, 14718.
- (22) (a) Grau, M. M.; Poizat, M.; Arends, I. W. C. E.; Hollmann, F. *Appl. Organomet. Chem.* **2010**, *24*, 380. (b) Hu, Y.; Norton, J. R. *J. Am. Chem. Soc.* **2014**, *136*, 5938.
- (23) (a) Chakraborty, S.; Brennessel, W. W.; Jones, W. D. *J. Am. Chem. Soc.* **2014**, *136*, 8564. (b) Bonitatibus, P. J., Jr.; Chakraborty, S.; Doherty, M. D.; Siclovan, O.; Jones, W. D.; Soloveichik, G. L. *Proc. Natl. Acad. Sci. U. S. A.* **2015**, *112*, 1687. (c) Morris, R. H. *Acc. Chem. Res.* **2015**, *48*, 1494. (d) Chakraborty, S.; Bhattacharya, P.; Dai, H.; Guan, H. *Acc. Chem. Res.* **2015**, *48*, 1995.
- (24) (a) Bauer, I.; Knölker, H.-J. *Chem. Rev.* **2015**, *115*, 3170. (b) Morris, R. H. *Chem. Soc. Rev.* **2009**, *38*, 2282. (c) Quintard, A.; Rodriguez, J. *Angew. Chem., Int. Ed.* **2014**, *53*, 4044. (d) Zhang, L.; Peng, D.; Leng, X.; Huang, Z. *Angew. Chem., Int. Ed.* **2013**, *52*, 3676. (e) Creutz, S. E.; Peters, J. C. *J. Am. Chem. Soc.* **2014**, *136*, 1105. (f) Rittle, J.; Peters, J. C. *Proc. Natl. Acad. Sci. U. S. A.* **2013**, *110*, 15898. (g) Chu, W.-Y.; Zhou, X.; Rauchfuss, T. B. *Organometallics* **2015**, *34*, 1619.
- (25) Wang, W.; Rauchfuss, T. B.; Zhu, L.; Zampella, G. *J. Am. Chem. Soc.* **2014**, *136*, 5773.
- (26) (a) Roger, C.; Hamon, P.; Toupet, L.; Rabaa, H.; Saillard, J. Y.; Hamon, J. R.; Lapinte, C. *Organometallics* **1991**, *10*, 1045. (b) Belkova, N. V.; Revin, P. O.; Epstein, L. M.; Vorontsov, E. V.; Bakhmutov, V. I.; Shubina, E. S.; Collange, E.; Poli, R. *J. Am. Chem. Soc.* **2003**, *125*, 11106.
- (27) Caughey, W. S.; Schellenberg, K. A. *J. Org. Chem.* **1966**, *31*, 1978.
- (28) (a) Ryan, O. B.; Tilset, M.; Parker, V. D. *J. Am. Chem. Soc.* **1990**, *112*, 2618. (b) Ryan, O. B.; Tilset, M.; Parker, V. D. *Organometallics* **1991**, *10*, 298.
- (29) (a) Klingler, R. J.; Huffman, J. C.; Kochi, J. K. *J. Am. Chem. Soc.* **1980**, *102*, 208. (b) Costello, M. T.; Walton, R. A. *Inorg. Chem.* **1988**, *27*, 2563.
- (30) (a) Rhodes, L. F.; Zubkowski, J. D.; Folting, K.; Huffman, J. C.; Caulton, K. G. *Inorg. Chem.* **1982**, *21*, 4185. (b) Detty, M. R.; Jones, W. D. *J. Am. Chem. Soc.* **1987**, *109*, 5666.
- (31) (a) Lemmen, T. H.; Lundquist, E. G.; Rhodes, L. F.; Sutherland, B. R.; Westerberg, D. E.; Caulton, K. G. *Inorg. Chem.* **1986**, *25*, 3915.
- (32) Hamon, P.; Toupet, L.; Hamon, J. R.; Lapinte, C. *Organometallics* **1992**, *11*, 1429.
- (33) Hamon, P.; Hamon, J.-R.; Lapinte, C. *J. Chem. Soc., Chem. Commun.* **1992**, 1602.
- (34) Cheng, J.-P.; Lu, Y.; Zhu, X.-Q.; Mu, L.-J. *J. Org. Chem.* **1998**, *63*, 6108.
- (35) Yuasa, J.; Yamada, S.; Fukuzumi, S. *Angew. Chem., Int. Ed.* **2008**, *47*, 1068.
- (36) (a) Paul, C. E.; Arends, I. W. C. E.; Hollmann, F. *Org. Lett.* **2013**, *15*, 180. (b) Zhu, X.-Q.; Tan, Y.; Cao, C.-T. *J. Phys. Chem. B* **2010**, *114*, 2058.
- (37) Fukuzumi, S.; Tokuda, Y.; Kitano, T.; Okamoto, T.; Otera, J. *J. Am. Chem. Soc.* **1993**, *115*, 8960.
- (38) (a) Catheline, D.; Astruc, D. *Organometallics* **1984**, *3*, 1094. (b) Walter, M. D.; White, P. S. *New J. Chem.* **2011**, *35*, 1842.